

Monte-Carlo generator for e^+e^- annihilation into lepton and hadron pairs with precise radiative corrections

A.B. Arbuzov¹, G.V. Fedotov², F.V. Ignatov²,
E.A. Kuraev¹, A.L. Sibidanov²

¹ *Bogoliubov Laboratory of Theoretical Physics, JINR,
Dubna, 141980, Russia*

² *Budker Institute for Nuclear Physics,
Prospect Lavrent'eva, 11, Novosibirsk, 630090, Russia*

Abstract

Recently, various cross sections of e^+e^- annihilation into hadrons were accurately measured in the energy range from 0.37 to 1.39 GeV with the CMD-2 detector at the VEPP-2M collider. In the $\pi^+\pi^-$ channel a systematic uncertainty of 0.6% has been achieved. A Monte-Carlo Generator Photon Jets (MCGPJ) was developed to simulate events of the Bhabha scattering as well as production of two charged pions, kaons and muons. Based on the formalism of Structure Functions, the leading logarithmic contributions related to the emission of photon jets in the collinear region are incorporated into the MC generator. Radiative corrections (RC) in the first order of α are accounted for exactly. The theoretical precision of the cross sections with RC is estimated to be better than 0.2%. Numerous tests of the program as well as comparison with other MC generators and CMD-2 experimental data are presented.

1 Introduction

The cross sections of e^+e^- annihilation into hadrons are very important in various problems of particle physics and, in particular, they are required for the evaluation of the hadronic contribution to the anomalous magnetic moment of muon, $a_\mu = (g - 2)_\mu/2$. The recent measurement of a_μ at BNL [1] led to a new world average differing by 2.7 standard deviations from its theoretical evaluation. One of the main ingredients in the theoretical prediction for a_μ is the hadronic contribution related via a dispersion integral to the cross section of e^+e^- annihilation into hadrons. In the case of a_μ^{had} , the VEPP-2M energy range gives the major contribution both to the hadronic vacuum polarization contribution itself and to its uncertainty [2, 3]. This uncertainty is dominated by systematic errors of the experimental values of $R(s)$ which are used as an input to the integral with the proper kernel function [4]:

$$a_\mu^{had} = \left(\frac{\alpha m_\mu}{3\pi}\right)^2 \int_{4m_\pi^2}^{\infty} \frac{R(s)K(s)}{s^2} ds.$$

The quantity $R(s)$ is defined as $R(s) = \sigma(e^+e^- \rightarrow \text{hadrons})/\sigma(e^+e^- \rightarrow \mu^+\mu^-)$ and at high energies can be calculated within the QCD framework whereas at low energies the experimental data are required. A numerical computation of this integral can be found elsewhere[2] and in relative unities its evaluation yields the result ~ 70 ppm.

The goal of the new BNL experiment [5] is to measure the anomalous magnetic moment of muon with the relative accuracy ~ 0.25 ppm. To reduce the current systematic error of the hadronic contribution to a_μ^{had} at least to the same level, the theoretical precision of the cross sections with radiative corrections (RC) should be better than 0.3% as it follows from a simple estimation: $70 \text{ ppm} \times 0.3\% \sim 0.2 \text{ ppm}$. This short observation shows why the knowledge of the cross sections e^+e^- annihilation into hadrons with high precision is extremely important.

The detection efficiency, background conditions and criteria of event selection from the raw data differ for specific e^+e^- annihilation modes. Therefore, expressions for the cross sections with RC on which the MC generator is based, should have a completely differential form with respect to the kinematic variables of final particles. In this case the influence of the selection criteria as well as the trigger efficiency and many other specific resolutions of the detector can be naturally incorporated in a MC generator.

During the last thirty years considerable efforts were devoted to elucidate theoretical understanding of the accuracy of cross sections with RC, particularly in the case of e^+e^- and $\pi^+\pi^-$ pair production at low energies. The radiatively corrected cross sections for annihilation channels with an accuracy of about 0.1% were obtained in [6]. Unfortunately, expressions for these cross sections do not contain the angular distributions for the emitted photons and, as a result, it is not possible to reconstruct the kinematics of the final particles correctly. On the other hand, the differential cross sections were obtained in [7], but their relative accuracy is about 1%, since only $\mathcal{O}(\alpha)$ QED corrections were taken into account.

The work [8] is based in part on a combination of the approaches [6, 7] mentioned above. To achieve the accuracy $\sim 0.2\%$, higher order radiative corrections were taken into account by means of the Structure Function (SF) formalism [6]. It involves a convolution of the *boosted* Born cross section with the electron (positron) SF, which describes the leading effects due to emission of photons in the collinear region as well as radiation of e^+e^- pairs. These enhanced contributions are proportional to $(\alpha/\pi)^n \ln^n(s/m_e^2)$, $n = 1, 2, \dots$ and are referred to as the leading ones. Moreover, in the *smoothed* representations of the SF [6] a certain part of these corrections is exponentiated and evaluated in all powers of n . The non-leading contributions proportional to (α/π) are incorporated exactly according to [6] by means of a so-called *K-factor*. The next-to-leading contributions of the second order $(\alpha/\pi)^2 \ln(s/m_e^2) \sim 0.01\%$ are fortunately small and can be omitted, keeping in mind the intended precision tag 0.2%.

The vacuum polarization effects in the photon propagator are treated as in [8] for the lepton channels. These effects are not included in RC for the hadronic modes according to the generally accepted agreement [10]. The emission of one hard photon at a large angle is described by a differential formula, which allows to take into account specific experimental conditions and cuts. Based on numerical calculations, which will be given below, it was established that the $\mathcal{O}(\alpha)$ radiative corrections together with photon jet radiation in a collinear region are sufficient to achieve a relative precision of the cross sections about $\sim 0.2\%$.

The purpose of this paper is to describe the Monte-Carlo Generator Photon Jets (MCGPJ) which simulates processes $e^+e^- \rightarrow e^+e^-, \mu^+\mu^-, \pi^+\pi^-, K^+K^-$ and $K_L K_S$. This generator was used while CMD-2 experimental data were processed. The MCGPJ code has a modular structure that simplifies the implementation of additional hadronic modes as well as the replacement

of matrix elements of the current cross sections by a new one. The effects of the final state radiation (FSR) for the channels $\mu^+\mu^-$, $\pi^+\pi^-$, K^+K^- have been incorporated into the program. The pions were assumed to be point-like objects, and the scalar QED was applied to calculate virtual, soft and hard photon emission by charged pions (kaons).

The relevant formulae for the cross sections with RC of order α are collected here from many other papers. It is done specially to have a possibility of quantifying the difference between cross sections due to radiation of one photon and photon jets in the collinear region. On the other hand, some expressions for RC are revisited in the present paper and explicit analytical formulae will be presented in the form convenient for the MC generator construction.

2 Monte-Carlo generator for events of Bhabha scattering at large angles

The *boosted* Born cross section of the process $e^-(z_1p_-) + e^+(z_2p_+) \rightarrow e^-(p_1) + e^+(p_2)$, corrected for vacuum polarization factors in the s and t channels, when initial particles lose some energy by radiation of photon jets in the collinear region, has the following form [8] in the c.m. frame:

$$\begin{aligned} \frac{d\tilde{\sigma}_0^{e^+e^- \rightarrow e^+e^-}(z_1, z_2)}{d\Omega_1} &= \frac{4z_1z_2\alpha^2}{a^2\tilde{s}} \left(\frac{\tilde{s}^2 + \tilde{u}^2}{2\tilde{t}^2|1 - \Pi(\tilde{t})|^2} + \frac{\tilde{t}^2 + \tilde{u}^2}{2\tilde{s}^2|1 - \Pi(\tilde{s})|^2} \right. \\ &\left. + \Re \left\{ \frac{\tilde{u}^2}{\tilde{s}\tilde{t}} \frac{1}{(1 - \Pi(\tilde{s}))(1 - \Pi(\tilde{t}))} \right\} \right), \end{aligned} \quad (1)$$

where z_1 and z_2 are the electron and positron fraction energies after radiation of photon jets ($z_{1,2} = \varepsilon_{1,2}/\varepsilon_{beam}$), $\Pi(\tilde{s})$ and $\Pi(\tilde{t})$ are the vacuum polarization operators in photon propagators in the s and t channels, respectively. The Mandelstam variables in the Lab and c.m.s. are defined as usual: $s = 2p_-p_+$, $t = -2p_-p_1$, $u = -2p_-p_2$, $\tilde{s} = sz_1z_2$, $\tilde{t} = -sz_1Y_1(1 - c_1)/2$, $\tilde{u} = -sz_2Y_1(1 + c_1)/2$, $s_1 = 2p_1p_2$, $t_1 = -2p_+p_2$, $u_1 = -2p_+p_2$, $c_1 = \cos\theta_1$, where θ_1 is a polar angle of the final electron with respect to the electron beam direction, Y_1 and Y_2 are the relative energies of final e^- and e^+ . The energy-momentum conservation law allows to reconstruct the kinematics of final particles and to find these energies and a positron polar angle θ_2 : $z_1 + z_2 = Y_1 + Y_2$ - energy conservation; $z_1 - z_2 = Y_1 \cos\theta_1 + Y_2 \cos\theta_2$ - momentum conservation along the Z-axis; $Y_1 \sin\theta_1 = Y_2 \sin\theta_2$ - momentum conservation in the plane perpendicular to the Z-axis. From these equations one can find that

$$\begin{aligned} Y_1 &= \frac{2z_1z_2}{a}, & Y_2 &= \frac{(z_1^2 + z_2^2) - (z_1^2 - z_2^2)c_1}{a}, \\ c_2 &= \frac{(z_1^2 - z_2^2) - (z_1^2 + z_2^2)c_1}{(z_1^2 + z_2^2) - (z_1^2 - z_2^2)c_1}, \end{aligned} \quad \text{where } a = z_1 + z_2 - (z_1 - z_2)c_1. \quad (2)$$

The expression for the differential cross section with one photon emission in the reaction $e^-(p_-) + e^+(p_+) \rightarrow e^-(p_1) + e^+(p_2) + \gamma(k)$, was obtained in [7] (see also references therein) and reads

$$d\sigma_{hard}^{e^+e^- \rightarrow e^+e^- \gamma} = \frac{\alpha^3}{2\pi^2 s} R_{hard}^{e^+e^- \rightarrow e^+e^- \gamma} \frac{d^3p_1}{\varepsilon_1} \frac{d^3p_2}{\varepsilon_2} \frac{d^3k}{\omega} \delta^{(4)}(p_- + p_+ - p_1 - p_2 - k), \quad (3)$$

where ε_1 , ε_2 , and ω are the energies of the final state electron, positron and photon, respectively; δ -function provides the energy-momentum conservation.

The expression for the quantity $R_{hard}^{e^+e^- \rightarrow e^+e^- \gamma}$ which contains the vacuum polarization effects in photon propagators was derived in [8]:

$$\begin{aligned}
R_{hard}^{e^+e^- \rightarrow e^+e^- \gamma} = & \frac{(WT)_\Pi}{4} \\
& - \frac{m_e^2}{\chi_+^2} \left(\frac{s^2 + (s+t)^2}{2t^2(1-\Pi(t))^2} + \frac{t^2 + (s+t)^2}{2s^2|1-\Pi(s)|^2} + \Re \left\{ \frac{(s+t)^2}{st(1-\Pi(s))(1-\Pi(t))} \right\} \right) \\
& - \frac{m_e^2}{\chi_-^2} \left(\frac{s^2 + (s+t_1)^2}{2t_1^2(1-\Pi(t_1))^2} + \frac{t_1^2 + (s+t_1)^2}{2s^2|1-\Pi(s)|^2} + \Re \left\{ \frac{(s+t_1)^2}{st_1(1-\Pi(s))(1-\Pi(t_1))} \right\} \right) \\
& - \frac{m_e^2}{\chi_+^2} \left(\frac{s_1^2 + (s_1+t)^2}{2t^2(1-\Pi(t))^2} + \frac{t^2 + (s_1+t)^2}{2s_1^2|1-\Pi(s_1)|^2} + \Re \left\{ \frac{(s_1+t)^2}{s_1t(1-\Pi(s_1))(1-\Pi(t))} \right\} \right) \\
& - \frac{m_e^2}{\chi_-^2} \left(\frac{s_1^2 + (s_1+t_1)^2}{2t_1^2(1-\Pi(t_1))^2} + \frac{t_1^2 + (s_1+t_1)^2}{2s_1^2|1-\Pi(s_1)|^2} + \Re \left\{ \frac{(s_1+t_1)^2}{s_1t_1(1-\Pi(s_1))(1-\Pi(t_1))} \right\} \right), \quad (4)
\end{aligned}$$

where $\chi_\pm = kp_\pm$ and $\chi'_\pm = kp_{1,2}$. The quantity $(WT)_\Pi$ describes the process with one hard photon emission and gives the dominant contribution outside the collinear region [8]:

$$\begin{aligned}
(WT)_\Pi = & \frac{SS}{|1-\Pi(s)|^2 s \chi'_- \chi'_+} + \frac{S_1 S_1}{|1-\Pi(s_1)|^2 s_1 \chi_- \chi_+} - \frac{TT}{|1-\Pi(t)|^2 t \chi_+ \chi'_+} \\
& - \frac{T_1 T_1}{|1-\Pi(t_1)|^2 t_1 \chi_- \chi'_-} + \Re \left[\frac{TT_1}{(1-\Pi(t))(1-\Pi(t_1)) t t_1 \chi_- \chi'_- \chi_+ \chi'_+} \right. \\
& - \frac{SS_1}{(1-\Pi(s))(1-\Pi(s_1))^* s s_1 \chi_- \chi'_- \chi_+ \chi'_+} + \frac{TS}{(1-\Pi(t))(1-\Pi(s)) t s \chi'_- \chi_+ \chi'_+} \\
& + \frac{T_1 S_1}{(1-\Pi(t_1))(1-\Pi(s_1)) t_1 s_1 \chi_- \chi'_- \chi_+} - \frac{T_1 S}{(1-\Pi(t_1))(1-\Pi(s)) t_1 s \chi_- \chi'_- \chi'_+} \\
& \left. - \frac{TS_1}{(1-\Pi(\tilde{t}))(1-\Pi(\tilde{s}_1)) t s_1 \chi_- \chi_+ \chi'_+} \right], \quad (5)
\end{aligned}$$

where the following notations were used:

$$\begin{aligned}
SS = S_1 S_1 &= t^2 + t_1^2 + u^2 + u_1^2, \\
TT = T_1 T_1 &= s^2 + s_1^2 + u^2 + u_1^2, \\
SS_1 &= (t^2 + t_1^2 + u^2 + u_1^2) \times (t \chi_+ \chi'_+ + t_1 \chi_- \chi'_- - u \chi_+ \chi'_- - u_1 \chi_- \chi'_+), \\
TT_1 &= (s^2 + s_1^2 + u^2 + u_1^2) \times (u \chi_+ \chi'_- + u_1 \chi_- \chi'_+ + s \chi'_- \chi'_+ + s_1 \chi_- \chi_+), \\
TS &= -\frac{1}{2}(u^2 + u_1^2)(s(t + s_1) + t(s + t_1) - uu_1), \\
TS_1 &= -\frac{1}{2}(u^2 + u_1^2)(t(s_1 + t_1) + s_1(s + t) - uu_1), \\
T_1 S &= \frac{1}{2}(u^2 + u_1^2)(t_1(s + t) + s(s_1 + t_1) - uu_1), \\
T_1 S_1 &= \frac{1}{2}(u^2 + u_1^2)(s_1(s + t_1) + t_1(s_1 + t) - uu_1). \quad (6)
\end{aligned}$$

The main contribution to the cross section due to photon radiation comes from the collinear region, where the cross section exhibits very steep behavior [11]. The collinear region is a part of the angular phase-space with four narrow cones (Fig. 1) surrounding the directions of motion

of the initial and final particles. The emitted photon should be inside these cones with an angle $2\theta_0$. The angle θ_0 should obey to the follow restrictions, $1/\gamma \ll \theta_0 \ll 1$, where $\gamma = \varepsilon/m_e$. It serves as an auxiliary parameter and usually its value is taken at about $\sim 1/\sqrt{7}$. The cross section integrated inside these narrow cones according to [8] is:

$$\begin{aligned} \frac{d\sigma_{\text{coll}}^{e^+e^- \rightarrow e^+e^- \gamma}}{d\Omega_1} &= \frac{\alpha}{\pi} \int_{\Delta}^1 \frac{dx}{x} \left\{ 2 \frac{d\tilde{\sigma}_0^{e^+e^- \rightarrow e^+e^-}(1,1)}{d\Omega_1} \left[\left(z + \frac{x^2}{2} \right) \left(L - 1 + \ln \frac{\theta_0^2 z^2}{4} \right) + \frac{x^2}{2} \right] \right. \\ &+ \left. \left[\frac{d\tilde{\sigma}_0^{e^+e^- \rightarrow e^+e^-}(z,1)}{d\Omega_1} + \frac{d\tilde{\sigma}_0^{e^+e^- \rightarrow e^+e^-}(1,z)}{d\Omega_1} \right] \left[\left(z + \frac{x^2}{2} \right) \left(L - 1 + \ln \frac{\theta_0^2}{4} \right) + \frac{x^2}{2} \right] \right\}, \quad (7) \end{aligned}$$

where $L = \ln(s/m_e^2)$, $z = 1 - x$ and the *boosted* Born cross section is defined in Eq. (1). The auxiliary parameter $\Delta = \Delta\varepsilon/\varepsilon$ ($\Delta \ll 1$) serves as a separator of hard and soft photons, ε is the beam energy. The terms proportional to $(\alpha/\pi)(L-1)$ are accounted for in the SF [6] and therefore should be removed from this expression to eliminate the double counting.

The remaining four terms can be interpreted as the so-called *compensators* which cancel out the dependence of the total cross section on the auxiliary parameter θ_0 when they are summed with the cross section Eq.(3) describing one hard photon emission outside cones.

Collecting all the discussed above terms into one formula we get the complete expression for the *master* formula describing the process $e^+e^- \rightarrow e^+e^- + n\gamma$, which can be presented as:

$$\begin{aligned} \frac{d\sigma^{e^+e^- \rightarrow e^+e^- + n\gamma}}{d\Omega_1} &= \int_0^1 dx_1 \int_0^1 dx_2 \int_0^1 dx_3 \int_0^1 dx_4 \frac{d\tilde{\sigma}_0^{e^+e^- \rightarrow e^+e^-}(z_1, z_2)}{d\Omega_1} \\ &\times \mathcal{D}(z_1, s) \mathcal{D}(z_2, s) \mathcal{D}(z_3, \tilde{s}) \mathcal{D}(z_4, \tilde{s}) \left(1 + \frac{\alpha}{\pi} \tilde{K}_{SV} \right) \Theta(\text{cuts}) \\ &+ \frac{\alpha}{\pi} \int_{\Delta}^1 \frac{dx_1}{x_1} \left[\left(z_1 + \frac{x_1^2}{2} \right) \ln \frac{\theta_0^2}{4} + \frac{x_1^2}{2} \right] \frac{d\tilde{\sigma}_0^{e^+e^- \rightarrow e^+e^-}(z_1, 1)}{d\Omega_1} \Theta(\text{cuts}) \\ &+ \frac{\alpha}{\pi} \int_{\Delta}^1 \frac{dx_2}{x_2} \left[\left(z_2 + \frac{x_2^2}{2} \right) \ln \frac{\theta_0^2}{4} + \frac{x_2^2}{2} \right] \frac{d\tilde{\sigma}_0^{e^+e^- \rightarrow e^+e^-}(1, z_2)}{d\Omega_1} \Theta(\text{cuts}) \\ &+ \frac{\alpha}{\pi} \int_{\Delta}^1 \frac{dx_3}{x_3} \left[\left(z_3 + \frac{x_3^2}{2} \right) \ln \frac{\theta_0^2 z_3^2}{4} + \frac{x_3^2}{2} \right] \frac{d\tilde{\sigma}_0^{e^+e^- \rightarrow e^+e^-}(1, 1)}{d\Omega_1} \Theta(\text{cuts}) \\ &+ \frac{\alpha}{\pi} \int_{\Delta}^1 \frac{dx_4}{x_4} \left[\left(z_4 + \frac{x_4^2}{2} \right) \ln \frac{\theta_0^2 z_4^2}{4} + \frac{x_4^2}{2} \right] \frac{d\tilde{\sigma}_0^{e^+e^- \rightarrow e^+e^-}(1, 1)}{d\Omega_1} \Theta(\text{cuts}) \\ &+ \frac{4\alpha}{\pi} \frac{d\tilde{\sigma}_0^{e^+e^- \rightarrow e^+e^-}(1, 1)}{d\Omega_1} \ln \frac{u}{t} \ln \Delta + \frac{\alpha^3}{2\pi^2 s} \int_{\substack{k^0 > \Delta\varepsilon \\ \theta_\gamma > \theta_0}} R_{\text{hard}}^{e^+e^- \rightarrow e^+e^- \gamma} \frac{d\Gamma}{d\Omega_1} \Theta(\text{cuts}), \quad (8) \end{aligned}$$

where $x_{1,2,3,4}$ are the relative energies of photon jets emitted along the initial and final particles; $z_{1,2,3,4} = 1 - x_{1,2,3,4}$ are the energy fractions of electrons and positrons after radiation of photon jets; $\Theta(\text{cuts})$ is a step-function equal to 1 (0) if the kinematics variables obey (or not) the selection criteria; the expression for $\tilde{K}_{SV}(\tilde{\theta}_1)$ can be found in [7, 8]. More details concerning the implementation of the SF formalism as adopted in the present paper can be found in [6].

The SF approach provides essential improvement of accuracy for the Bhabha cross section by taking into account radiation of photon jets in the collinear region. These improvements as well as others performed in [8] are summarized below:

1. The radiation of photon jets (enhanced contributions) is taken into account by means of the SF formalism.
2. To combine the cross sections, describing radiation of one hard photon inside and outside narrow cones, the four *compensators* are embedded into the *master* formula (Eq.8).
3. The *boosted* Born cross section contributes to the total cross section in conformity with SF weights in the *master* formula (Eq.8).
4. The vacuum polarization effects inserted into all photon propagators exactly.
5. Non-leading contributions of order α are accounted for by means of the so-called *K-factor*.

The integration limits of the first term in Eq.8 were divided in two parts from 0 to $\Delta\varepsilon$ and from $\Delta\varepsilon$ to the maximal jet energy. As a result, the four-fold integral splits into sixteen parts. Those of them with one photon jet radiation are merged in a proper way with *compensators* in the *master* formula. In this case, the total cross section is subdivided into seventeen cross sections with own specific kinematics - number of photon jets and directions of their radiation. The first contribution accounting for effects due to soft and virtual radiative corrections is given by

$$\begin{aligned} \frac{d\sigma_1^{e^+e^- \rightarrow e^+e^- + n\gamma}}{d\Omega_1} &= \int_0^\Delta \int_0^\Delta \int_0^\Delta \int_0^\Delta dx_1 dx_2 dx_3 dx_4 \mathcal{D}(z_1, s) \mathcal{D}(z_2, s) \mathcal{D}(z_3, \tilde{s}) \mathcal{D}(z_4, \tilde{s}) \\ &\times \left(1 + \frac{\alpha}{\pi} \tilde{K}_{SV}\right) \frac{d\tilde{\sigma}_0^{e^+e^- \rightarrow e^+e^-}(z_1, z_2)}{d\Omega_1} - \frac{4\alpha}{\pi} \ln\left(\frac{u}{t}\right) \ln \Delta \frac{d\tilde{\sigma}_0^{e^+e^- \rightarrow e^+e^-}(1, 1)}{d\Omega_1}. \end{aligned} \quad (9)$$

The photon jet energy emitted by each charged particle can be up to $\Delta\varepsilon$. This part also contains the contribution due to production of virtual and soft real e^+e^- pairs if $2m_e < \Delta\varepsilon$.

The next four terms represent the contribution to the cross section with one hard jet emission along the motion of any charged particle, supplied with the virtual and soft leading logarithmic corrections. One of these terms with the relevant *compensator* is:

$$\begin{aligned} \frac{d\sigma_2^{e^+e^- \rightarrow e^+e^- + n\gamma}}{d\Omega_1} &= \int_\Delta^1 \int_0^\Delta \int_0^\Delta \int_0^\Delta dx_1 dx_2 dx_3 dx_4 \mathcal{D}(z_2, s) \mathcal{D}(z_3, \tilde{s}) \mathcal{D}(z_4, \tilde{s}) \frac{d\tilde{\sigma}_0^{e^+e^- \rightarrow e^+e^-}(z_1, z_2)}{d\Omega_1} \\ &\left[\mathcal{D}(z_1, s) \left(1 + \frac{\alpha}{\pi} \tilde{K}_{SV}\right) + \frac{\alpha}{\pi} \frac{1}{x_1} \left(\left(z_1 + \frac{x_1^2}{2}\right) \ln \frac{\theta_0^2}{4} + \frac{x_1^2}{2} \right) \right] \Theta(\text{cuts}). \end{aligned} \quad (10)$$

The other similar terms can be written out in the same way by the permutation of limits between integrals.

The next six terms represent the contribution to the cross section when two jets are emitted simultaneously along momenta of any two charged particles. One of these terms reads

$$\begin{aligned} \frac{d\sigma_6^{e^+e^- \rightarrow e^+e^- + n\gamma}}{d\Omega_1} &= \int_\Delta^1 \int_\Delta^1 \int_0^\Delta \int_0^\Delta dx_1 dx_2 dx_3 dx_4 \mathcal{D}(z_1, s) \mathcal{D}(z_2, s) \mathcal{D}(z_3, \tilde{s}) \mathcal{D}(z_4, \tilde{s}) \\ &\times \frac{d\tilde{\sigma}_0^{e^+e^- \rightarrow e^+e^-}(z_1, z_2)}{d\Omega_1} \left(1 + \frac{\alpha}{\pi} \tilde{K}_{SV}\right) \Theta(\text{cuts}). \end{aligned} \quad (11)$$

The other similar terms have the identical structure and are obtained by the limits permutation.

The following four terms represent the contribution to the cross section when three photon jets are emitted along momenta of any three charged particles. One of these terms is given by

$$\begin{aligned} \frac{d\sigma_{12}^{e^+e^- \rightarrow e^+e^- + n\gamma}}{d\Omega_1} &= \int_{\Delta}^1 \int_{\Delta}^1 \int_{\Delta}^1 \int_0^{\Delta} dx_1 dx_2 dx_3 dx_4 \mathcal{D}(z_1, s) \mathcal{D}(z_2, s) \mathcal{D}(z_3, \tilde{s}) \mathcal{D}(z_4, \tilde{s}) \\ &\times \frac{d\tilde{\sigma}_0^{e^+e^- \rightarrow e^+e^-}(z_1, z_2)}{d\Omega_1} \left(1 + \frac{\alpha}{\pi} \tilde{K}_{SV}\right) \Theta(\text{cuts}). \end{aligned} \quad (12)$$

The cross section with emission of four jets along the momenta of each initial and final particle is written below,

$$\begin{aligned} \frac{d\sigma_{16}^{e^+e^- \rightarrow e^+e^- + n\gamma}}{d\Omega_1} &= \int_{\Delta}^1 \int_{\Delta}^1 \int_{\Delta}^1 \int_{\Delta}^1 dx_1 dx_2 dx_3 dx_4 \mathcal{D}(z_1, s) \mathcal{D}(z_2, s) \mathcal{D}(z_3, \tilde{s}) \mathcal{D}(z_4, \tilde{s}) \\ &\times \frac{d\tilde{\sigma}_0^{e^+e^- \rightarrow e^+e^-}(z_1, z_2)}{d\Omega_1} \left(1 + \frac{\alpha}{\pi} \tilde{K}_{SV}\right) \Theta(\text{cuts}). \end{aligned} \quad (13)$$

The cross section with one hard photon emission outside the collinear region reads

$$\frac{d\sigma_{17}^{e^+e^- \rightarrow e^+e^- \gamma}}{d\Omega_1} = \frac{\alpha^3}{2\pi^2 s} \int_{\substack{k^0 > \Delta\varepsilon \\ \theta_\gamma > \theta_0}} R_{hard}^{e^+e^- \rightarrow e^+e^- + \gamma} \frac{sx_1 x dx d\Omega_\gamma}{8(1 - x \sin^2 \psi/2)} \Theta(\text{cuts}), \quad (14)$$

where ψ is an angle between the momenta directions of photon and final electron.

The cross section calculation was performed by the Monte-Carlo method. The cutoff energy $\Delta\varepsilon$ was chosen at ten electron masses to optimise the efficiency of event simulation ($\Delta = \Delta\varepsilon/\varepsilon \sim 1\%$). Since the *master* formula is singular on some variables, the main of them have been isolated: photon energy and emission angle were generated according to functions $1/\omega(\varepsilon - \omega)$ and $1/(1 - \beta_e^2 \cos^2 \theta_\gamma)$, respectively. The main contribution to the Bhabha cross section comes from the t channel and it was generated by the function $1/(1 - \cos \theta_1)^2$.

The selection criteria adopted here for the simulated events are similar to those used in CMD-2 data analysis [3] and they are:

the acollinearity cut in the scattering plane is $|\Delta\theta| < 0.25$ rad, where $\Delta\theta = \theta_1 + \theta_2 - \pi$;
the same for azimuthal plane, $|\Delta\phi| < 0.15$ rad, where $\Delta\phi = |\phi_1 - \phi_2| - \pi$;
the angular acceptance is $1.1 < \theta_{\text{aver}} < \pi - 1.1$, where $\theta_{\text{aver}} = (\theta_1 - \theta_2 + \pi)/2$; $p_{1,2}^\perp > 90$ MeV/c.
Below, if nothing specially told about selection criteria the latter will be taken in mind.

The MCGPJ program consists of two main stages. In the first stage with a soft selection criteria all majorants for seventeen parts are determined, in the second one the cross sections with experimental selection criteria are being determined. The generator simulates an event according to specific kinematics for each cross section. The weight of event is determined as the ratio of a given cross section (one from seventeen) to the total one. The kinematic parameters of the simulated events are stored in the proper histograms, which can be compared with experimental distributions.

Numerous tests have been performed for the c.m.s. energy of 900 MeV. The cross section dependence on the auxiliary parameter $\Delta\varepsilon$ is shown in Fig.2 after integration over the remaining kinematic variables. It is seen that the cross section variations are inside the claimed precision while $\Delta\varepsilon$ changes by a factor of 10^4 . The cross section variations with an auxiliary parameter θ_0 do not exceed $\pm 0.1\%$ level (Fig.3). From that certainly follows that the cross section stability to the auxiliary parameters $\Delta\varepsilon$ and θ_0 at least is not worse than 0.1%.

Comparison of different kinematic distributions simulated by the MCGPJ generator and BHWIDE [12] was performed. Distributions over parameters $\Delta\theta = \theta_1 + \theta_2 - \pi$ and $\Delta\phi = |\phi_1 - \phi_2| - \pi$ are plotted in Figs.4, 5. Good agreement is seen while $\Delta\theta$ and $\Delta\phi$ vary in the wide range. Asymmetric shape of the distribution on $\Delta\phi$ is due to specific kinematic of the events, when photon and e^+e^- pair fly in diametrically opposed sides. The cross section for such kinematic has enhancement which visualizes as shape asymmetry of the distribution.

The event distributions produced by both generators are presented in Fig. 6 as a function of missing energy ($\varepsilon_{mis.} = 2\varepsilon - \varepsilon_1 - \varepsilon_2$). Both distributions are close to each other except for the energy region where soft and hard photons are merged. A visible bump is observed in this point. This bump originates from a slightly different dependence on the cutoff energy of both the *compensators* and the cross section with one hard photon. The cut on acollinearity $\Delta\theta \sim 0.25$ rad, is equivalent to missing energy ~ 100 MeV that is rather far from cutoff energy $\Delta\varepsilon \sim 7$ MeV. As a result, the contribution into the total cross section connected with this spurious features is negligible.

The relative difference of the cross sections, presented in Fig.7, calculated by the MCGPJ code and BHWIDE is less than 0.1% for the VEPP-2M energy range. This difference *versus* the acollinearity angle $\Delta\theta$ is plotted in Fig.8. One can see that the size and sign of the difference depend on the particular choice of $\Delta\theta$. The reason of the difference about $\sim 0.5\%$ for $\Delta\theta \sim 0.05$ rad arises from the fact that all photons (except one in our code) are emitted strongly along the motion of electrons (positrons) whereas in BHWIDE they have some angular distribution. The difference of $\sim 0.3\%$ for the large acollinearity angles $|\Delta\theta| \sim 1$ rad is due to the fact that the BHWIDE code simulates one hard photon only. It is worth noticing the MCGPJ code describes the shape of *tails* of the different kinematic distributions a bit correctly and, as a result, it is preferable for applications when *soft* selection criteria are used.

It is important to reliably estimate the total theoretical precision of this approach. In order to quantify a theoretical error, the independent comparison has been performed with the generator based on Ref. [7], where $\mathcal{O}(\alpha)$ QED corrections are treated exactly. It was found that the relative difference of cross sections is more than 1% for small acollinearity angles $\Delta\theta < 0.1$ rad (Fig. 9) and it is less than $\sim 0.2\%$ for acollinearity angles ~ 0.25 rad. From that immediately follows that the radiation of two and more photons (jets) in the collinear region contributes to the cross section by the amount $\sim 0.2\%$ only. Therefore, we can conclude that the theoretical precision of the Bhabha cross section with RC is certainly better than $\sim 0.2\%$ for our selection criteria.

The EM calorimeter of the CMD-2 detector allows to separate Bhabha scattering events from others with high confidence level [3]. The distributions in acollinearity angles $\Delta\theta$ and $\Delta\phi$ are presented in Figs.10,11. To increase the experimental statistics, all the CMD-2 data at energies greater than 1040 MeV collected in these plots. The momentum and angular resolutions, interaction with the detector material were added to the kinematic parameters of simulated events. The histograms were fitted by two Gaussian functions. Their relative weights and widths were fit parameters. Good agreement between experiment and simulation

can be seen.

The agreement between experiment and simulation becomes significantly worse when the MC generator based on Ref. [7] with $\mathcal{O}(\alpha)$ corrections is used. It is seen in Figs.12,13 where two-dimensional plots are presented. The points in these plots correspond to the electron and positron energies. Different population of events is observed far aside from the area where *semi-elastic* events are concentrated. About $\sim 1\%$ events have correlated low energies and they are distributed predominantly along a corridor which extends from the right upper to the left bottom corner of this plot. The appearance of these events is due to simultaneous radiation of two jets with close energies along either initial or final particles. The condition $p_{1,2}^\perp > 90$ MeV/c is very soft and only owing to this fact the integrated cross sections are equal to each other within $\sim 0.2\%$. If $p_{1,2}^\perp$ is about ~ 220 MeV/c, the relative difference increases up to $\sim 1\%$ (Fig.14). For the values $p_{1,2}^\perp$ more than 350 MeV/c the difference changes a sign and grows up. The cross section with photon jets becomes smaller than with one photon under condition $p_{1,2}^\perp > 350$ MeV/c. This feature has a simple explanation. The distribution width of *semi-elastic* events in the first plot is broader than for the second one due to radiation of many soft photons and, as a result, these events are *smeared* more broadly near the peak area.

3 Monte-Carlo generator for production of muon pairs

The same approach was used to create the MC generator to simulate production of muon pairs in the reaction $e^-(z_1 p_-) + e^+(z_2 p_+) \rightarrow \mu^-(p_1) + \mu^+(p_2)$, when initial particles radiate some energy by emission of photon jets in the collinear region. According to [8] the *boosted* Born cross section modified by the vacuum polarization effects in the photon propagator reads

$$\frac{d\tilde{\sigma}_0^{e^+e^- \rightarrow \mu^+\mu^-}(z_1, z_2)}{d\Omega_1} = \frac{\alpha^2}{4s} \frac{1}{|1 - \Pi(z_1 z_2 s)|^2} \frac{y_1 [z_1^2 (Y_1 - y_1 c_1)^2 + z_2^2 (Y_1 + y_1 c_1)^2 + 8z_1 z_2 m_\mu^2 / s]}{z_1^3 z_2^3 [z_1 + z_2 - (z_1 - z_2) c_1 Y_1 / y_1]}, \quad (15)$$

where $y_{1,2}^2 = Y_{1,2}^2 - 4m_\mu^2/s$; $Y_{1,2} = \varepsilon_{1,2}/\varepsilon$ are the muon relative energies; $z_{1,2} = 1 - x_{1,2}$, $x_{1,2} = \omega_{1,2}/\varepsilon$ are the relative energies of photon jets; $c_1 = \cos\theta_1$, θ_1 is a polar angle of negative muon. The energy-momentum conservation law,

$$z_1 + z_2 = Y_1 + Y_2, \quad z_1 - z_2 = y_1 c_1 + y_2 c_2, \quad y_1 \sqrt{1 - c_1^2} = y_2 \sqrt{1 - c_2^2},$$

allows to determine Y_1 , Y_2 and a positron polar angle θ_2 ($c_2 = \cos\theta_2$):

$$Y_1 = \frac{2m_\mu^2}{s} \frac{(z_2 - z_1)c_1}{z_1 z_2 + [z_1^2 z_2^2 - (m_\mu^2/s)((z_1 + z_2)^2 - (z_1 - z_2)^2 c_1^2)]^{1/2}} + \frac{2z_1 z_2}{z_1 + z_2 - c_1(z_1 - z_2)}. \quad (16)$$

The charge-even part of the cross section in the first order in α comes from one-loop virtual (V) and soft (S) radiative corrections and according to Ref. [13] is given by:

$$\frac{d\sigma_{even}^{S+V}}{d\Omega_1} = \frac{d\tilde{\sigma}_0^{e^+e^- \rightarrow \mu^+\mu^-}(1, 1)}{d\Omega_1} \frac{2\alpha}{\pi} (A_e + A_\mu),$$

$$A_e = (L - 1) \ln \frac{\Delta\varepsilon}{\varepsilon} + \frac{3}{4}(L - 1) + \frac{\pi^2}{6} - \frac{1}{4}, \quad A_\mu = \left(\frac{1 + \beta^2}{2\beta} \ln \frac{1 + \beta}{1 - \beta} - 1 \right) \ln \frac{\Delta\varepsilon}{\varepsilon} + K_{even}^\mu. \quad (17)$$

The expression for the quantity K_{even}^μ was derived in [14] and reads

$$\begin{aligned}
K_{\text{even}}^\mu &= -1 + \rho \left(\frac{1 + \beta^2}{2\beta} - \frac{1}{2} + \frac{1}{4\beta} \right) + \ln \frac{1 + \beta}{2} \left(\frac{1}{2\beta} + \frac{1 + \beta^2}{\beta} \right) \\
&\quad - \frac{1 - \beta^2}{2\beta} \frac{l_\beta}{2 - \beta^2(1 - c_1^2)} + \frac{1 + \beta^2}{2\beta} \left[\frac{\pi^2}{6} + 2\text{Li}_2 \left(\frac{1 - \beta}{1 + \beta} \right) + l_\beta \ln \frac{1 + \beta}{2\beta^2} \right], \\
l_\beta &= \ln \frac{1 + \beta}{1 - \beta}, \quad \rho = \ln \frac{s}{m_\mu^2}, \quad L = \ln \frac{s}{m_e^2}, \quad \text{Li}_2(x) \equiv - \int_0^x \frac{dt}{t} \ln(1 - t). \quad (18)
\end{aligned}$$

In the ultra relativistic limit ($\beta \rightarrow 1$) the quantity A_μ takes the same form as for electrons

$$A_\mu = (L_\mu - 1) \ln \frac{\Delta\varepsilon}{\varepsilon} + \frac{3}{4}(L_\mu - 1) + \frac{\pi^2}{6} - \frac{1}{4}. \quad (19)$$

The charge-odd part of the cross section comes from the interference of the Born amplitude with box-type diagrams as well as with amplitudes of soft photon emission by initial and final particles and is given by [14, 8]:

$$\begin{aligned}
\frac{d\sigma_{\text{odd}}^{S+V}}{d\Omega_1} &= \frac{d\sigma_0^{e^+e^- \rightarrow \mu^+\mu^-}}{d\Omega_1} (1, 1) \frac{2\alpha}{\pi} \left(2 \ln \frac{\Delta\varepsilon}{\varepsilon} \ln \frac{1 - \beta c_1}{1 + \beta c_1} + K_{\text{odd}}^\mu \right), \\
K_{\text{odd}}^\mu &= \frac{1}{2} l_-^2 - L_-(\rho + l_-) + \text{Li}_2 \left(\frac{1 - \beta^2}{2(1 - \beta c_1)} \right) + \text{Li}_2 \left(\frac{\beta^2(1 - c_1^2)}{1 + \beta^2 - 2\beta c_1} \right) \\
&\quad - \int_0^{1-\beta^2} \frac{dx}{x} f(x) \left(1 - \frac{x(1 + \beta^2 - 2\beta c_1)}{(1 - \beta c_1)^2} \right)^{-\frac{1}{2}} + \frac{1}{2 - \beta^2(1 - c_1^2)} \\
&\quad \times \left\{ -\frac{1 - 2\beta^2 + \beta^2 c_1^2}{1 + \beta^2 - 2\beta c_1} (\rho + l_-) - \frac{1}{4} (1 - \beta^2) \left[l_-^2 - 2L_-(l_- + \rho) \right. \right. \\
&\quad \left. \left. + 2\text{Li}_2 \left(\frac{1 - \beta^2}{2(1 - \beta c_1)} \right) \right] + \beta c_1 \left[-\frac{\rho}{2\beta^2} + \left(\frac{\pi^2}{12} + \frac{1}{4}\rho^2 \right) \left(1 - \frac{1}{\beta} - \frac{\beta}{2} + \frac{1}{2\beta^3} \right) \right. \right. \\
&\quad \left. \left. + \frac{1}{\beta} \left(-1 - \frac{\beta^2}{2} + \frac{1}{2\beta^2} \right) \left(\rho \ln \frac{1 + \beta}{2} - 2\text{Li}_2 \left(\frac{1 - \beta}{2} \right) - \text{Li}_2 \left(-\frac{1 - \beta}{1 + \beta} \right) \right) \right. \right. \\
&\quad \left. \left. - \frac{1}{2} l_-^2 + L_-(\rho + l_-) - \text{Li}_2 \left(\frac{1 - \beta^2}{2(1 - \beta c_1)} \right) \right] \right\} - (c_1 \rightarrow -c_1), \quad (20) \\
f(x) &= \left(\frac{1}{\sqrt{1-x}} - 1 \right) \ln \frac{\sqrt{x}}{2} - \frac{1}{\sqrt{1-x}} \ln \frac{1 + \sqrt{1-x}}{2}, \\
l_- &= \ln \frac{1 - \beta c_1}{2}, \quad L_- = \ln \left(1 - \frac{1 - \beta^2}{2(1 - \beta c_1)} \right).
\end{aligned}$$

For the ultra relativistic limit the same result as in [14] is obtained.

The cross section of muon pair production with one hard photon emission is studied in detail elsewhere [13, 8]. This cross section in the differential form, keeping the relevant information about the kinematics of final particles, can be written as:

$$d\sigma_{\text{hard}}^{e^+e^- \rightarrow \mu^+\mu^-\gamma} = \frac{\alpha^3}{2\pi^2 s^2} R_{\text{hard}}^{e^+e^- \rightarrow \mu^+\mu^-\gamma} \frac{s\beta_1 d\Omega_1 dx d\Omega_\gamma}{4[2 - x(1 - \cos \psi/\beta_1)]}, \quad (21)$$

where β_1 is a velocity of negative muon. The quantity $R_{\text{hard}}^{e^+e^- \rightarrow \mu^+\mu^-\gamma}$ consists of three terms and represents the cross section with one hard photon emitted by the initial and final particles as well as their interference:

$$\begin{aligned}
R_{\text{hard}}^{e^+e^- \rightarrow \mu^+\mu^-\gamma} &= \frac{s}{16(4\pi\alpha)^3} \sum_{\text{spins}} |M|^2 = R_{ee} + R_{e\mu} + R_{\mu\mu}, \tag{22} \\
R_{ee} &= \frac{1}{|1 - \Pi(s_1)|^2} \left[C \frac{s}{\chi_- \chi_+} + \frac{m_\mu^2}{s_1^2} \Delta_{s_1 s_1} - \frac{m_e^2}{2\chi_-^2} \frac{(t_1^2 + u_1^2 + 2m_\mu^2 s_1)}{s_1^2} - \frac{m_e^2}{2\chi_+^2} \frac{(t^2 + u^2 + 2m_\mu^2 s_1)}{s_1^2} \right], \\
R_{e\mu} &= \Re \frac{1}{(1 - \Pi(s_1))(1 - \Pi(s))^*} \left[C \left(\frac{u}{\chi_- \chi'_+} + \frac{u_1}{\chi_+ \chi'_-} - \frac{t}{\chi_- \chi'_-} - \frac{t_1}{\chi_+ \chi'_+} \right) + \frac{m_\mu^2}{s s_1} \Delta_{s s_1} \right] \\
R_{\mu\mu} &= \frac{1}{|1 - \Pi(s)|^2} \left[\frac{s_1}{\chi'_- \chi'_+} C + \frac{m_\mu^2}{s^2} \Delta_{ss} \right], \quad C = \frac{u^2 + u_1^2 + t^2 + t_1^2}{4s s_1}, \\
\Delta_{s_1 s_1} &= \frac{(t+u)^2 + (t_1+u_1)^2}{2\chi_- \chi_+}, \quad \Delta_{ss} = -\frac{u^2 + t_1^2 + 2sm_\mu^2}{2(\chi'_-)^2} - \frac{u_1^2 + t^2 + 2sm_\mu^2}{2(\chi'_+)^2} \\
&\quad + \frac{(s s_1 - s^2 + tu + t_1 u_1 - 2sm_\mu^2)}{\chi'_- \chi'_+}, \\
\Delta_{s s_1} &= \frac{s + s_1}{2} \left(\frac{u}{\chi_- \chi'_+} + \frac{u_1}{\chi_+ \chi'_-} - \frac{t}{\chi_- \chi'_-} - \frac{t_1}{\chi_+ \chi'_+} \right) + \frac{2(u - t_1)}{\chi'_-} + \frac{2(u_1 - t)}{\chi'_+}.
\end{aligned}$$

Mandelstam variables and χ_\pm, χ'_\pm are defined as for electrons. Similar to the Bhabha cross section, the *master* formula describing the process of muon pair production reads [8]

$$\begin{aligned}
\frac{d\sigma^{e^+e^- \rightarrow \mu^+\mu^- + n\gamma}}{d\Omega_1} &= \int_0^1 \int_0^1 dx_1 dx_2 \mathcal{D}(z_1, s) \mathcal{D}(z_2, s) \frac{d\tilde{\sigma}_0^{e^+e^- \rightarrow \mu^+\mu^-}(z_1, z_2)}{d\Omega_1} \left(1 + \frac{2\alpha}{\pi} \tilde{K} \right) \Theta(\text{cuts}) \\
&\quad + \frac{\alpha}{\pi} \int_{\Delta}^1 \frac{dx_1}{x_1} \left[\left(z_1 + \frac{x_1^2}{2} \right) \ln \frac{\theta_0^2}{4} + \frac{x_1^2}{2} \right] \frac{d\tilde{\sigma}_0^{e^+e^- \rightarrow \mu^+\mu^-}(z_1, 1)}{d\Omega_1} \Theta(\text{cuts}) \\
&\quad + \frac{\alpha}{\pi} \int_{\Delta}^1 \frac{dx_2}{x_2} \left[\left(z_2 + \frac{x_2^2}{2} \right) \ln \frac{\theta_0^2}{4} + \frac{x_2^2}{2} \right] \frac{d\tilde{\sigma}_0^{e^+e^- \rightarrow \mu^+\mu^-}(1, z_2)}{d\Omega_1} \Theta(\text{cuts}) \\
&\quad + \frac{\alpha^3}{2\pi^2 s^2} \int_{\substack{k^0 > \Delta\varepsilon \\ \theta_\gamma > \theta_0}} R_{\text{hard}}^{e^+e^- \rightarrow \mu^+\mu^-\gamma} \frac{s\beta_1 x dx d\Omega_\gamma}{4[2 - x(1 - \cos\psi/\beta_1)]} \Theta(\text{cuts}) \\
&\quad + \frac{2\alpha}{\pi} \left[\frac{1 + \beta^2}{2\beta} \ln \frac{1 + \beta}{1 - \beta} - 1 + 2 \ln \frac{1 - \beta c_1}{1 + \beta c_1} \right] \ln\left(\frac{\Delta\varepsilon}{\varepsilon}\right) \cdot \frac{d\tilde{\sigma}_0^{e^+e^- \rightarrow \mu^+\mu^-}(1, 1)}{d\Omega_1} \Theta(\text{cuts}), \tag{23}
\end{aligned}$$

where $\tilde{K} = \pi^2/6 - 1/4 + K_{\text{even}}^\mu(\tilde{s}, \tilde{\theta}_1) + K_{\text{odd}}^\mu(\tilde{s}, \tilde{\theta}_1)$ and $\tilde{\theta}_1$ is a polar angle of negative muon in the c.m.frame. The *master* formula drawn above provides within the scope of the discussion the intended cross section accuracy $\sim 0.2\%$. The integration limits of the first term in Eq.23 were divided into two parts as for electrons. A two-fold integral splits into four separate contributions. Those of them which describe one photon jet radiation are combined in a proper way with two *compensators* in the *master* formula. All other steps to construct the MC generator to simulate production of muon pair are similar to that as for electrons and can be found in [16].

Numerical comparisons with the KKMC [15] generator have been performed. The theoretical accuracy of the formulae on which KKMC is based is about $\sim 0.1\%$. The existing code in KKMC does not provide the correct description of vacuum polarization effects in the photon propagator at low energies, so they were switched off in both generators. The relative difference between cross sections calculated with the MCGPJ generator and KKMC in the VEPP-2M energy range is presented in Fig.15. Good agreement at the level of our precision $\pm 0.2\%$ is observed.

In the low energy range, the momentum resolution of the CMD-2 detector is sufficient to distinguish pions, muons and electrons. Thus we have a direct way to compare the number of selected muons to that of electrons divided by the ratio of the theoretical cross sections, $\sigma(ee \rightarrow \mu\mu)/\sigma(ee \rightarrow ee)$ and check thereby the theoretical precision of the formulae with RC from experiment. The results for this double ratio are presented in Fig.16. One can see that a deviation from unity of the double ratio does not exceed on average 1.4% with statistical and systematic errors about $\sim 1.5\%$ and $\sim 0.7\%$, respectively. The scarce experimental statistics in this energy range does not allow to make the comparison with better accuracy.

4 Monte-Carlo generator for production of pion pairs

The same ideas as for muons were applied here to construct the *master* formula to the processes $e^+e^- \rightarrow \pi^+\pi^-(n\gamma)$, $K^+K^-(n\gamma)$, $K_S K_L(n\gamma)$, assuming that pseudo scalar mesons are point-like objects. The enhanced contributions to the cross section, coming from the collinear region, are accounted for by means of SF formalism. The one-loop virtual corrections, radiation of soft as well as one hard photon are taken into account in the first order of α exactly. The effects of the vacuum polarization are not included into the formulae presented below. In this case we deal with the so-called *dressed* cross section, when the dynamics of the pions strong interaction is encoded in the form factor properties. But, the Coulomb interaction in the final state should be included into RC to eliminate electromagnetic corrections.

According to the papers [9, 16] the *boosted* Born cross section is given by the expression

$$\frac{d\tilde{\sigma}_0^{e^+e^- \rightarrow \pi^+\pi^-}(z_1, z_2)}{d\Omega_1} = \frac{\alpha^2 (Y_1^2 - m_\pi^2/\varepsilon^2)^{3/2}}{4s} \frac{(1 - c_1^2) |F_\pi(s z_1 z_2)|^2}{z_1^2 z_2^2 (z_1 + z_2 + (z_2 - z_1)(1 - m_\pi^2/(\varepsilon^2 Y_1^2))^{-1/2} c_1)}, \quad (24)$$

where $z_{1,2}$ are the energy fractions of the electron and positron after radiation of photon jets in the collinear region, $|F_\pi(s z_1 z_2)|^2$ is a pion form factor squared, $c_1 = \cos\theta_1$, θ_1 is a polar angle between momentum of negative pion and electron beam direction. The energy fractions $Y_{1,2}$ of the final pions and the polar angle of the positive pion, θ_2 , can be found from the same kinematic relations as for muons.

The charge-even part of the cross section due to radiation of soft and virtual photons [17, 18] can be written in a convenient way as in [9]:

$$\frac{d\sigma_{\text{even}}^{S+V}}{d\Omega_1} = \frac{d\sigma_0^{e^+e^- \rightarrow \pi^+\pi^-}(1, 1)}{d\Omega_1} \cdot \frac{2\alpha}{\pi} (A_e + A_\pi),$$

$$A_e = (L - 1) \ln \frac{\Delta\varepsilon}{\varepsilon} + \frac{3}{4}(L - 1) + \frac{\pi^2}{6} - \frac{1}{4}, \quad A_\pi = \left(\frac{1 + \beta^2}{2\beta} \ln \frac{1 + \beta}{1 - \beta} - 1 \right) \ln \frac{\Delta\varepsilon}{\varepsilon} + K_{\text{even}}^\pi. \quad (25)$$

The expression for the quantity K_{even}^π can be found in [9, 18].

$$K_{\text{even}}^\pi = -1 + \frac{1-\beta}{2\beta}\rho + \frac{2+\beta^2}{\beta}\ln\frac{1+\beta}{2} + \frac{1+\beta^2}{2\beta}\left[\rho + \frac{\pi^2}{6} + l_\beta\ln\frac{1+\beta^2}{2\beta^2} + 2\text{Li}_2\frac{1-\beta}{1+\beta}\right]. \quad (26)$$

The charge-odd part of the differential cross section is the interference result of the Born amplitude with those describing box-type diagrams and soft photons emission by electrons and pions [19]. According to [9] the expression for the charge-odd part has the following form:

$$\frac{d\sigma_{\text{odd}}^{S+V}}{d\Omega_1} = \frac{d\sigma_0^{e^+e^-\rightarrow\pi^+\pi^-}(1,1)}{d\Omega_1} \cdot \frac{2\alpha}{\pi}\left(2\ln\frac{\Delta\varepsilon}{\varepsilon}\ln\frac{1-\beta c_1}{1+\beta c_1} + K_{\text{odd}}^\pi\right), \quad (27)$$

where K_{odd}^π , in its turn, is equal to

$$K_{\text{odd}}^\pi = \frac{1}{2}l_-^2 - \text{Li}_2\left(\frac{1-2\beta c_1+\beta^2}{2(1-\beta c_1)}\right) + \text{Li}_2\left(\frac{\beta^2(1-c_1^2)}{1-2\beta c_1+\beta^2}\right) \quad (28)$$

$$\begin{aligned} & - \int_0^{1-\beta^2} \frac{dx}{x} f(x) \left(1 - \frac{x(1-2\beta c_1+\beta^2)}{(1-\beta c_1)^2}\right)^{-\frac{1}{2}} \\ & + \frac{1}{2\beta^2(1-c_1^2)} \left\{ \left[\frac{1}{2}l_-^2 - (L+l_-)L_- + \text{Li}_2\left(\frac{1-\beta^2}{2(1-\beta c_1)}\right) \right] (1-\beta^2) \right. \\ & + (1-\beta c_1) \left[-l_-^2 - 2\text{Li}_2\left(\frac{1-\beta^2}{2(1-\beta c_1)}\right) + 2(L+l_-)L_- \right. \\ & - \frac{(1-\beta)^2}{2\beta} \left(\frac{1}{2}L^2 + \frac{\pi^2}{6} \right) + \frac{1+\beta^2}{\beta} \left(L\ln\frac{2}{1+\beta} - \text{Li}_2\left(-\frac{1-\beta}{1+\beta}\right) \right. \\ & \left. \left. \left. + 2\text{Li}_2\left(\frac{1-\beta}{2}\right) \right) \right] \right\} - (c_1 \rightarrow -c_1), \quad (29) \end{aligned}$$

$$\begin{aligned} f(x) &= \left(\frac{1}{\sqrt{1-x}} - 1 \right) \ln \frac{\sqrt{x}}{2} - \frac{1}{\sqrt{1-x}} \ln \frac{1+\sqrt{1-x}}{2}, \\ l_- &= \ln \frac{1-\beta c_1}{2}, \quad L_- = \ln \left(1 - \frac{1-\beta^2}{2(1-\beta c_1)} \right). \end{aligned}$$

The cross section of pion pair production accompanied by hard photon emission can be presented in the following form [9]:

$$\frac{d\sigma_{\text{hard}}^{e^+e^-\rightarrow\pi^+\pi^-\gamma}}{d\Omega_1} = \frac{\alpha^3}{32\pi^2 s} R_{\text{hard}}^{e^+e^-\rightarrow\pi^+\pi^-\gamma} \frac{s\beta_1 x dx d\Omega_\gamma}{4[2-x(1-\cos\psi/\beta_1)]}. \quad (30)$$

The quantity $R_{\text{hard}}^{e^+e^-\rightarrow\pi^+\pi^-\gamma}$ contains the terms describing initial and final state radiation and their interference:

$$\begin{aligned} R_{\text{hard}}^{e^+e^-\rightarrow\pi^+\pi^-\gamma} &= R_{ee} + R_{\pi\pi} + R_{e\pi}, \\ R_{ee} &= |F_\pi(s_1)|^2 \left\{ A \frac{4s}{\chi_-\chi_+} - \frac{8m_e^2}{s_1^2} \left(\frac{t_1 u_1}{\chi_-^2} + \frac{t u}{\chi_+^2} \right) + \frac{8m_e^2 m_\pi^2}{s_1} \left(\frac{1}{\chi_-^2} + \frac{1}{\chi_+^2} \right) + m_\pi^2 \Delta_{s_1 s_1} \right\}, \\ R_{\pi\pi} &= |F_\pi(s)|^2 \left\{ A \frac{4s_1}{\chi'_-\chi'_+} - \frac{8m_\pi^2}{s^2} \left(\frac{t u_1}{\chi_+'^2} + \frac{t_1 u}{\chi_-'^2} \right) + m_\pi^2 \Delta_{ss} \right\}, \end{aligned}$$

$$\begin{aligned}
R_{e\pi} &= \Re (F_\pi(s)F_\pi^*(s_1)) \left\{ 4A \left(\frac{u}{\chi_- \chi'_+} + \frac{u_1}{\chi_+ \chi'_-} - \frac{t}{\chi_- \chi'_-} - \frac{t_1}{\chi_+ \chi'_+} \right) + m_\pi^2 \Delta_{ss_1} \right\}, \\
A &= \frac{tu + t_1 u_1}{ss_1}, \quad \Delta_{s_1 s_1} = -\frac{4}{s_1^2} \frac{(t+u)^2 + (t_1+u_1)^2}{\chi_+ \chi_-}, \\
\Delta_{ss} &= \frac{2m_\pi^2 (s-s_1)^2}{s(\chi'_- \chi'_+)^2} + \frac{8}{s^2} (tt_1 + uu_1 - s^2 - ss_1), \\
\Delta_{ss_1} &= \frac{8}{ss_1} \left[\frac{2(t_1-u) + u_1 - t}{\chi'_-} + \frac{2(t-u_1) + u - t_1}{\chi'_+} \right. \\
&\quad \left. + \frac{u_1 + t_1 - s}{2\chi_-} \left(\frac{u}{\chi'_+} - \frac{t}{\chi'_-} \right) + \frac{u+t-s}{2\chi_+} \left(\frac{u_1}{\chi'_-} - \frac{t_1}{\chi'_+} \right) \right]. \tag{31}
\end{aligned}$$

Mandelstam variables and χ_\pm, χ'_\pm are defined as for electrons. The expression for the *master* formula, describing the process of pion pair production with two *compensators*, has a similar form as for muons and reads

$$\begin{aligned}
\frac{d\sigma^{e^+e^- \rightarrow \pi^+\pi^- + n\gamma}}{d\Omega_1} &= \int_0^1 \int_0^1 dx_1 dx_2 \mathcal{D}(z_1, s) \mathcal{D}(z_2, s) \frac{d\tilde{\sigma}_0^{e^+e^- \rightarrow \pi^+\pi^-}(z_1, z_2)}{d\Omega_1} \left(1 + \frac{2\alpha}{\pi} \tilde{K} \right) \Theta(\text{cuts}) \\
&+ \frac{\alpha}{\pi} \int_{\Delta}^1 \frac{dx_1}{x_1} \left[\left(z_1 + \frac{x_1^2}{2} \right) \ln \frac{\theta_0^2}{4} + \frac{x_1^2}{2} \right] \frac{d\tilde{\sigma}_0^{e^+e^- \rightarrow \pi^+\pi^-}(z_1, 1)}{d\Omega_1} \Theta(\text{cuts}) \\
&+ \frac{\alpha}{\pi} \int_{\Delta}^1 \frac{dx_2}{x_2} \left[\left(z_2 + \frac{x_2^2}{2} \right) \ln \frac{\theta_0^2}{4} + \frac{x_2^2}{2} \right] \frac{d\tilde{\sigma}_0^{e^+e^- \rightarrow \pi^+\pi^-}(1, z_2)}{d\Omega_1} \Theta(\text{cuts}) \\
&+ \frac{\alpha^3}{32\pi^2 s} \int_{\substack{k^0 > \Delta\varepsilon \\ \theta_\gamma > \theta_0}} R_{\text{hard}}^{e^+e^- \rightarrow \pi^+\pi^- \gamma} \frac{s\beta_1 x dx d\Omega_\gamma}{4[2-x(1-\cos\psi/\beta_1)]} \Theta(\text{cuts}) \\
&+ \frac{2\alpha}{\pi} \left[\frac{1+\beta^2}{2\beta} \ln \frac{1+\beta}{1-\beta} - 1 + 2 \ln \frac{1-\beta c_1}{1+\beta c_1} \right] \ln \frac{\Delta\varepsilon}{\varepsilon} \cdot \frac{d\tilde{\sigma}_0^{e^+e^- \rightarrow \pi^+\pi^-}(1, 1)}{d\Omega_1} \Theta(\text{cuts}), \tag{32}
\end{aligned}$$

where $\tilde{K} = \pi^2/6 - 1/4 + K_{\text{even}}^\pi(\tilde{s}, \tilde{\theta}_1) + K_{\text{odd}}^\pi(\tilde{s}, \tilde{\theta}_1)$, $\tilde{\theta}_1$ is a polar angle of negative pion in the center-of-mass system. As well as for muons, the integration limits with energy in the first term in Eq.32 were again divided in two parts. Two terms describing one photon jet radiation are merged with two *compensators*. Comparison with the BABAYAGA [20] generator was performed. The theoretical accuracy of the formulae, used in the BABAYAGA code, is about $\sim 1\%$. The current version of the BABAYAGA code (3.5) doesn't include the FSR and so this term was removed from our code (just for comparison). The difference of the cross sections calculated by the MCGPJ generator and BABAYAGA is shown in Fig.17 with the same selection criteria as for Bhabha scattering events. A systematic shift between cross sections is on average about 1% in agreement with the BABAYAGA code precision, but for the lowest and highest energies the agreement becomes worse.

The distributions of pion, muon and electron pairs as a function of momentum are presented in Fig.18 at the c.m.s. energy of 390 MeV for experimental and simulated events. Momentum and angle resolutions, decays in flight, interaction with the detector material and other important factors were *smear*ed with the parameters of simulated events to create events as close as possible to the *real* ones. The histograms for each type of particles were fitted by

two Gaussian functions. Their relative weights and widths were the free parameters of the fit. Perfect agreement between experiment and simulation one can see.

The enveloping curve describes pretty well the shape of histograms both at the *peaks* and at the *tails*. It permits to determine the number of events inside each histogram and to estimate the amount of the muons and electrons under the pion peak and thereby to extract the systematic error due to events separation procedure.

The shape of histograms peaks of the simulated events is not described well, if the MC generator, based on the formulae in the first order in α , is used. The shape of the histogram peak is mainly driven by the emission spectrum of soft photons and the apparatus resolution. Thus, the number of events in the *tail* area is determined by the peak shape and hence, the approach with photon jet radiation is absolutely necessary.

The MC generator simulating production of charged kaons is created similarly to that for pions. The pion mass m_π and form factor should be replaced in the above expressions by the kaon ones. The cross section being multiplied by the exact Coulomb factor will interpolate the energy dependence of the cross section from the threshold production to the relativistic region. The exact expression for the Coulomb factor was obtained by Sommerfeld-Sakharov and reads

$$f(z) = \frac{z}{1 - \exp(-z)} - z/2, \quad z = \frac{2\pi\alpha}{v} \quad (33)$$

where v is a relative velocity of kaons. The term $z/2$ is subtracted because it is already included in the $\mathcal{O}(\alpha)$ corrections to final state.

The MC generator simulating production of neutral kaons is significantly simpler since there is no Coulomb interaction and photon emission in the final state. The quantity $R_{\text{hard}}^{e^+e^- \rightarrow K_L K_S \gamma}$ (31) consists of one term which describes the initial state radiation only and the value \tilde{K} is equal to $\pi^2/6 - 1/4$.

5 Summary and concluding remarks

The MC generator for the processes $e^+e^- \rightarrow e^+e^-, \mu^+\mu^-, \pi^+\pi^-, K^+K^-$ and $K_L K_S$ is described in detail. An extended treatment of radiative corrections is implemented in the generator to get a high level of theoretical precision. The current version of the program, Monte-Carlo Generator Photon Jets (MCGPJ), includes radiation effects in the first order in α exactly. The corrections deal with radiation of hard photon decomposed into the three parts which describe initial and final state radiation and their interference. All terms in the matrix elements which are proportional to the muon or pion mass squared are kept. The enhanced contributions coming from the collinear region are accounted for by means of the SF formalism. As a result, the theoretical accuracy of the cross sections with RC is estimated to be at $\sim 0.2\%$ level. It is better by at least a factor of two compared to the accuracy $0.5 - 1\%$ achieved in earlier papers. Comparison with the well known codes BHWIDE, KKMC and BABAYAGA shows a satisfactory level of agreement for many distributions simulated by the generators.

The shape of the distributions with acollinearity angles $\Delta\theta$ and $\Delta\phi$ agrees with the CMD-2 experimental data. The double ratio of the number of muon events to that of electrons divided

by the ratio of the theoretical cross sections was found to be 0.986 ± 0.014 . The deviation from unity is $-1.4 \pm 1.4\%$. This is the first direct comparison of the experimental cross sections with the theoretical calculation at the accuracy $\sim 1\%$. The comparison of momenta distributions at the lowest energy point shows that only the simulation with radiation of photon jets describes the experimental spectra pretty well. Relying upon the above sketched review, the main conclusion is that theoretical predictions aiming at a $\mathcal{O}(0.1\%)$ precision must include contributions of both exact $\mathcal{O}(\alpha)$ terms and all higher order $\mathcal{O}(\alpha^n L^n)$ corrections.

The theoretical uncertainties of the cross sections with RC are determined by the unaccounted higher order corrections and they are estimated to be at $\sim 0.2\%$ level. Below, the main sources of uncertainties in the current formulae are listed:

- The weak interaction contributions are omitted in our approach. The numerical estimations show that for energies $2\varepsilon < 3$ GeV these contributions do not exceed 0.1% .
- A part of the second order next-to-leading radiative corrections proportional to $(\alpha/\pi)^2 L \sim 10^{-4}$ were omitted. Among these contributions are: the effect due to double photon emission (one inside and one outside of the narrow cone); emission of soft or virtual photon simultaneously with radiation of one hard photon at large angles. Even if we assume that a coefficient in front of these terms will be of order of ten, their contribution can not exceed $\sim 0.1\%$.
- The next source of uncertainties is related to the calculation of the hadronic vacuum polarization contribution to the photon propagator. Numerical estimations show that a systematic error of hadronic cross sections of about 1% changes the cross section by less than $\sim 0.04\%$.
- The uncertainty of about 0.1% is related to the theoretical models which are used to describe the energy dependence of the hadronic cross sections.
- In Ref. [21] it was concluded that a combined effect of all the parametrically enhanced $\mathcal{O}(\alpha^2)$ corrections can be numerically limited by 2.0×10^{-4} for near threshold production. The magnitude of this contribution slowly decreases with the final particle velocity β and therefore these corrections are beyond the intended accuracy.
- The last source of uncertainty is mainly driven by the collinear kinematic approximation. Several terms proportional to $(\alpha/\pi)\theta_0^2$ and $(\alpha/\pi)(1/\gamma\theta_0)^2$ were omitted. Numerical estimations show that the contribution of these factors is about $\sim 0.1\%$.

Considering the uncertainty sources mentioned above as independent, we can conclude that the total systematic error of the cross sections with RC is less than 0.2% . An indirect confirmation of the correct evaluation of the accuracy is the comparison of cross sections with RC calculated in the first order of α only. The corresponding difference does not exceed 0.2% . From that follows that higher order enhanced contributions, coming from collinear regions with emission of two and more photons, contribute to the cross section by amount of $\sim 0.2\%$ only for our selection criteria. Since the accuracy of this contribution is certainly known better than 100% , the systematic theoretical uncertainty for the cross sections with RC is $\sim 0.2\%$

The authors are grateful to V.S. Fadin, A.V. Bogdan, A.I. Milstein and G.N. Shestakov, to all members of the CMD-2 collaboration and particularly to S.I. Eidelman and B.I. Khazin for fruitful and useful discussions. We are also grateful to S. Jadach and W. Placzek for their help in running the BHWIDE and KKMC codes, G. Montagna and C.M. Carloni Calame for the useful collaboration on the BABAYAGA code.

This work is supported in part by the grants: RFBR-99-02-17053, RFBR-99-02-17119, RFBR-03-02-17077 and INTAS 96-0624.

References

- [1] G.V. Bennett *et al.*, Phys. Rev. Lett. **92** (2004) 161802.
- [2] S. Eidelman and F. Jegerlehner, Z. Physik C **67** (1995) 585,
M. Davier *et al.*, Eur. Phys. J. C **27** (2003) 497;
M. Davier, Nucl. Phys. B (Proc. Suppl.)**131** (2003) 192;
T. Teubner, Nucl. Phys. B (Proc. Suppl.)**131** (2003) 201;
M. Davier, S. Eidelman, A. Hocker and Z. Zhang, Eur. Phys. J. C **31** (2003) 503.
- [3] R.R. Akhmetshin *et al.*, Phys. Lett. B **89** (2002) 161;
R.R. Akhmetshin *et al.*, Nucl. Phys. B (Proc. Suppl.)**131** (2003) 3.
- [4] B. Lautrup, A. Peterman and E. de Rafael, Phys. Rep. **3** (1972) 193.
- [5] (g-2) Collaboration, Proposal E969, BNL (2004).
- [6] E.A. Kuraev and V.S. Fadin, Sov. J. Nucl. Phys.**41** (1985) 466;
S. Yadach, M. Skrzypek and B.F.L. Ward, Phys.Lett. B **257** (1991) 173;
M. Skrzypek, Acta Phys. Polon, B **23** (1992) 135.
M. Cacciari, A. Deandrea, G. Montagna and O. Nicrosini, Europhys. Lett. **17** (1992) 123;
A.B. Arbuzov *et al.*, JETP **81** (1995) 638;
A.B. Arbuzov *et al.*, Nucl. Phys. B **485** (1997) 457;
- [7] F.A. Berends *et al.*, Nucl. Phys. B **122** (1977) 485;
F.A. Berends *et al.*, Nucl. Phys. B **57** (1973) 381;
Erratum-ibid. B **75** (1974) 546;
F.A. Berends, K.J.F. Gaemers and R. Gastmans, Nucl. Phys. B **68** (1974) 541;
F.A. Berends and R. Kleiss, Nucl. Phys. B **228** (1983) 537;
S.I. Eidelman and E.A. Kuraev, Phys. Lett. B **80** (1978) 94.
- [8] A.B. Arbuzov *et al.*, JHEP **10** (1997) 001.
- [9] A.B. Arbuzov *et al.*, JHEP **10** (1997) 006.
- [10] Z. Jakubowski *et al.*, Z. Phys. C **40** (1988) 49;
Y.S. Tsay, SLAC - PUB - 1515 (1973).
- [11] V.N. Bayer, V.S. Fadin, V.A. Khoze, Nucl. Phys. B **65** (1973) 381.
- [12] S. Jadach, W. Placzek, B.F.L. Ward, Phys. Lett. B **390** (1997) 298.

- [13] V.N. Bayer and V.A. Khoze, JETP, vol.**48** (1965) 946;
S.I. Eidelman, E.A. Kuraev, V.S. Panin, Nucl. Phys. B **148** (1979) 245;
F.A. Berends *et al.*, Phys. Lett. B **103**, (1981) 124.
E.A. Kuraev, G.V. Meledin, Nucl. Phys. B **122** (1977) 485.
- [14] I.B. Khriplovich, Sov. J. Yad. Fiz, **17** (1973) 576;
D.A. Dicus, Phys. Rev. D **8** (1973) 890;
F.A. Berends and R. Kleiss, Nucl. Phys. B **177** (1981) 237.
- [15] S. Jadach *et al.*, Comp. Phys. Commun. **130** (2000) 260.
- [16] A.B. Arbuzov, G.V. Fedotovitch *et al.*, Preprint, BINP 2004-70
- [17] R.W. Brown and K.O. Mikaelian, Lett. Nuovo Cim. **10** (1974) 305.
- [18] A. Hofer, J. Gluza and F. Jegerlehner, Eur. Phys. J. C **24** (2002) 51.
- [19] V.N. Bayer, VIII Winter School LINP, v.II (1973) 164;
O.P. Sushkov, Sov. J. Yad. Fiz. **22** (1975) 868.
- [20] C.M. Carloni Calame *et al.*, Nucl. Phys **B584** (2000) 459;
C.M. Carloni Calame, Phys. Lett. **B520** (2001) 16.
- [21] M.B. Voloshin, Preprint, TPI-MINN-02/49-T, arXiv:hep-ph/021207, v1.

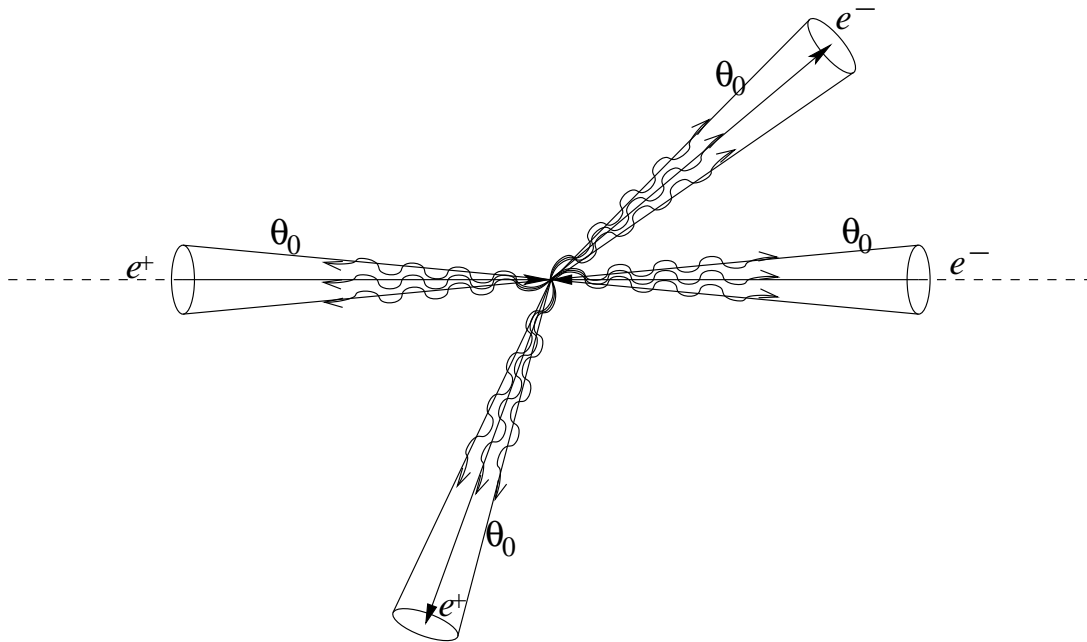


Figure 1: Photon jets are inside four narrow cones with an opening angle $2\theta_0$.

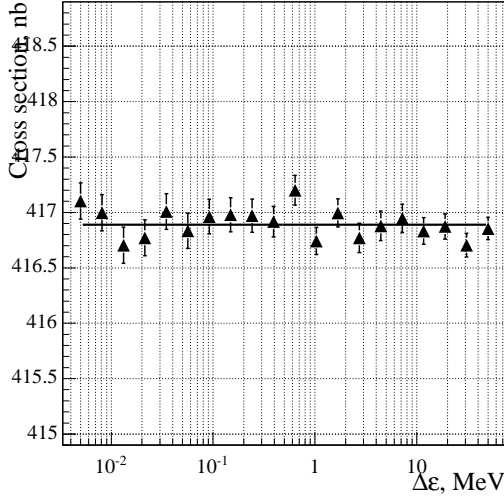


Figure 2: The cross section dependence on the auxiliary parameter $\Delta\varepsilon$. Parameters and selection cuts are given in text.

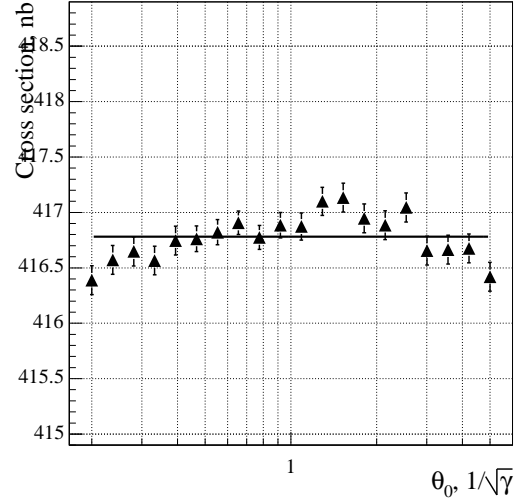


Figure 3: The cross section dependence on the auxiliary parameter θ_0 after integration over the remaining kinematic variables.

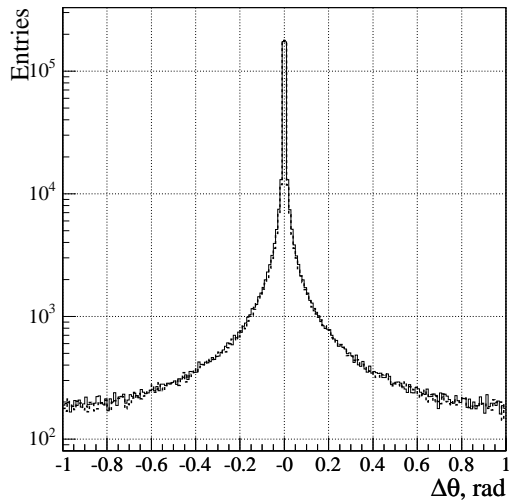


Figure 4: The acollinearity polar angle $\Delta\theta$ distribution. The solid line—MCGPJ code, the dashed line—BHWIDE.

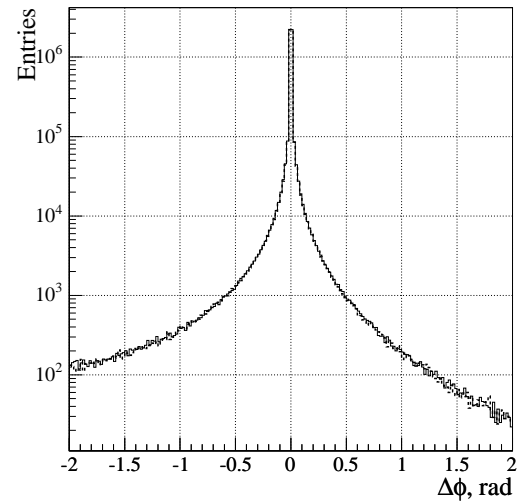


Figure 5: The acollinearity azimuthal angle $\Delta\phi$ distribution. The solid line – MCGPJ code, the dashed line – BHWIDE.

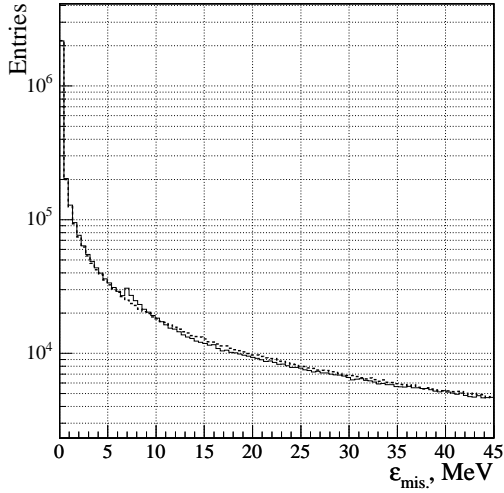


Figure 6: The distribution of events as a function of the missing energy radiated by electrons and positrons. The solid line – MCGPJ code, the dashed line – BHWIDE.

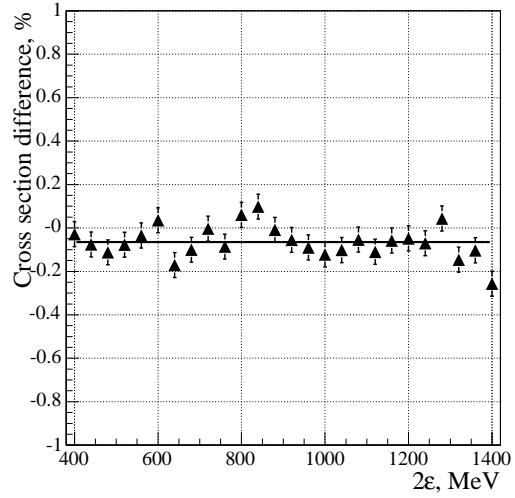


Figure 7: The relative difference of cross sections calculated by the MCGPJ code and BHWIDE as a function of the c.m.energy.

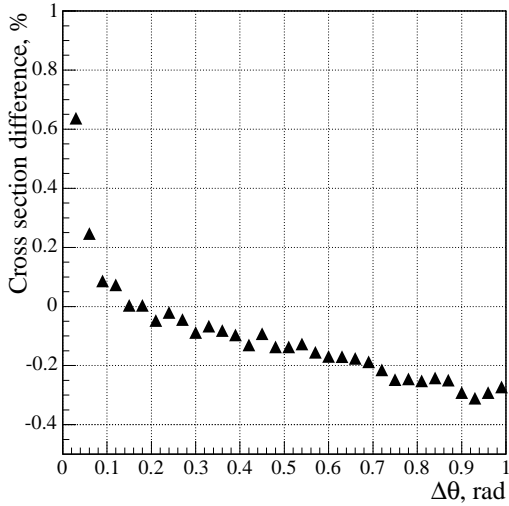


Figure 8: The relative difference between cross sections calculated by the MCGPJ code and BHWIDE *versus* the acollinearity angle $|\Delta\theta|$.

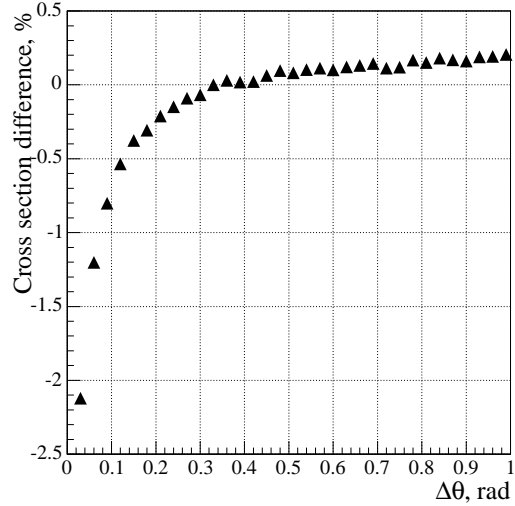


Figure 9: The relative difference between cross sections calculated by the MCGPJ code and the generator based on Ref. [7] *versus* the acollinearity angle $|\Delta\theta|$.

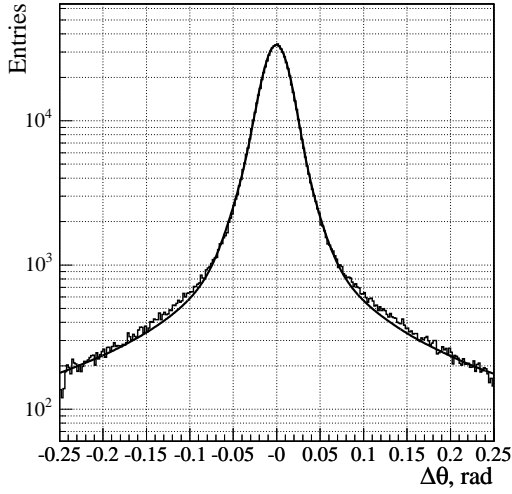


Figure 10: The acollinearity angle $\Delta\theta$ distribution in the scattering plane. Solid line - simulation, histogram - experiment.

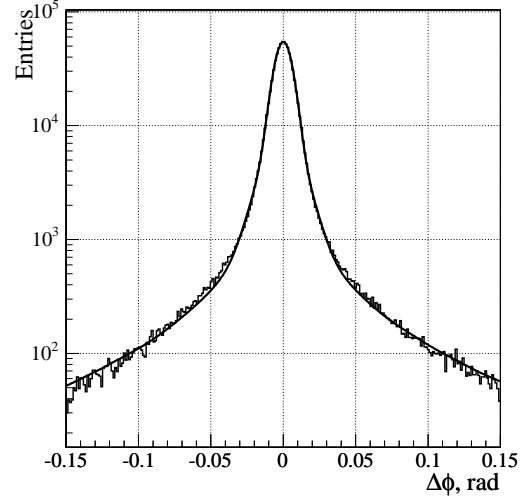


Figure 11: The acollinearity angle $\Delta\phi$ distribution in the azimuthal plane. Solid line - simulation, histogram - experiment.

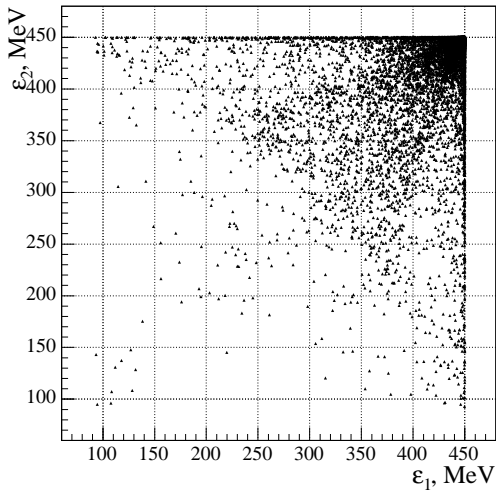


Figure 12: Two-dimensional plot of the simulated events (MCGPJ). The points in this plot correspond to the electron and positron energies. The influence of the condition $\Delta\theta < 0.25$ rad can be seen from an ark-like smooth border.

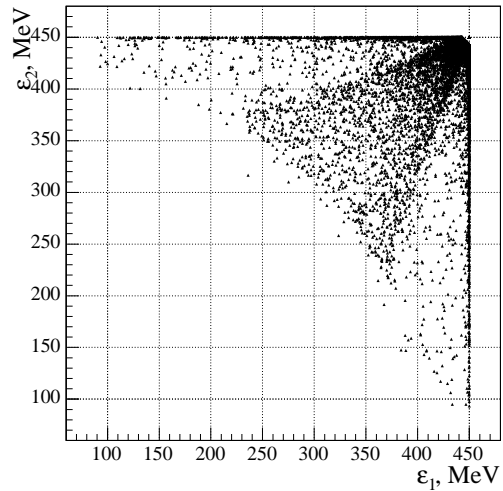


Figure 13: Two-dimensional plot of the simulated events. The generator is based on [7]. The points in this plot correspond to the electron and positron energies. The condition $\Delta\theta < 0.25$ rad divides the plot into two parts - with and without events.

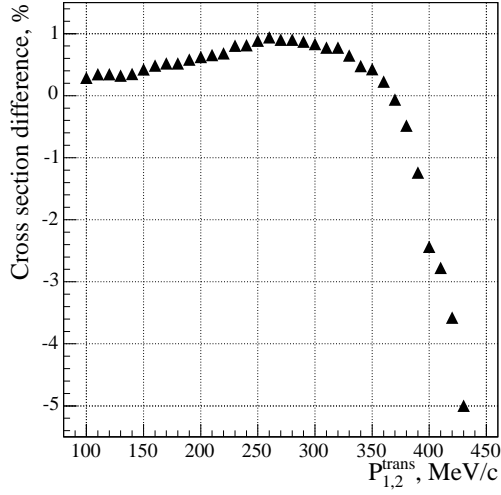


Figure 14: The difference between cross sections as a function of the cut imposed on the transverse momenta of final particles.

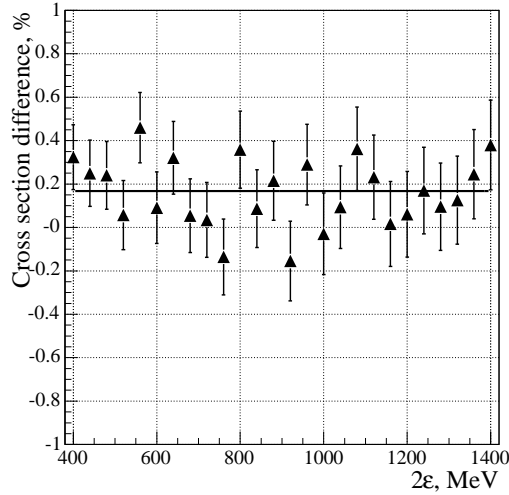


Figure 15: The relative difference between the cross sections calculated by the MCGPJ code and KKMC *versus* the c.m.energy.

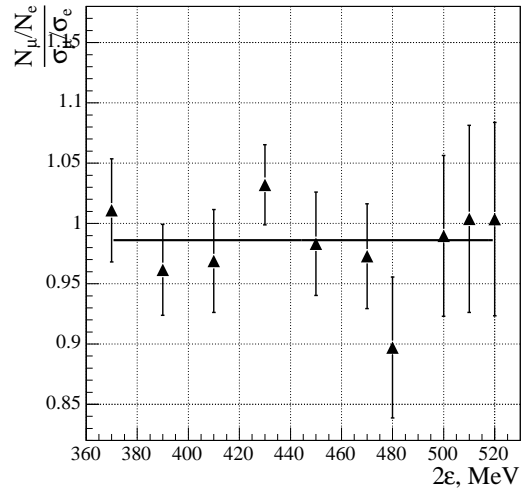


Figure 16: The ratio of the number of selected muons to that of electrons divided by the ratio of the corresponding theoretical cross sections.

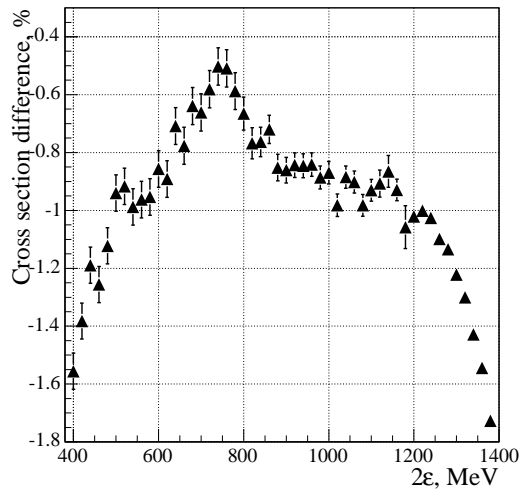


Figure 17: The relative difference between the cross sections calculated by the MCGPJ code and BABAYAGA *versus* the beam energy.

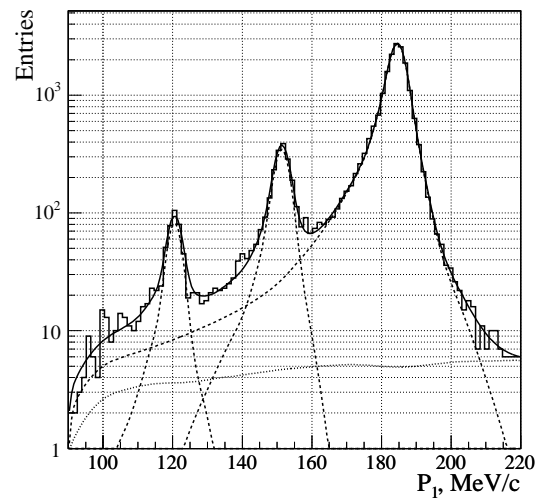


Figure 18: The distribution of pion, muon and electron pairs as a function of the momentum. The upper curve represents a common fit, bottom curve - mainly cosmic ray background.